SEMARAK ILMU PUBLISHING

Semarak Journal of Thermal-Fluid Engineering

Journal homepage:
https://semarakilmu.my/index.php/sjotfe/index
ISSN: 3030-6639

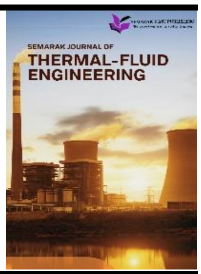

Comparative Study of Internal Flow Dynamics Using CFD: Flow through Sudden Pipe Contraction and Expansion

Mohd Haqeem Hadi Adam[1], Ishkrizat Taib[1,*]

[1] Department of Mechanical Engineering, Faculty of Engineering Mechanical and Manufacturing, Universiti Tun Hussein Onn Malaysia, Johor, Malaysia

ARTICLE INFO

Article history:
Received 26 April 2026
Received in revised form 5 May 2026
Accepted 22 May 2026
Available online 30 June 2026

Keywords:
Sudden pipe; contraction; expansion; CFD

ABSTRACT

Sudden changes in cross-sectional area are encountered by many engineering systems with internal fluid flows, such as fluid distribution networks, control valves, and industrial nozzles. These abrupt geometric transitions lead to complex hydrodynamic phenomena, predominantly severe flow separation, the generation of recirculation vortices and large variations in localised static pressure. In order to optimise the system performance and to minimise the mechanical energy losses, the pressure drop across the geometric irregularities should be predicted accurately. Hence, the present work is aimed to numerically investigate the internal flow behaviour and quantify the exact pressure drop in a horizontal pipe with a sudden contraction followed immediately by a sudden expansion. A 2D axisymmetric computational domain was developed and the incompressible Navier-Stokes, continuity and energy conservation equations were solved using a finite-volume method discretisation approach. The working fluid was liquid water and the inlet velocity was uniform at 0.125 m/s at the upstream boundary. In order to ensure that the numerical predictions were mathematically stable and not influenced by the spatial discretisation, a rigorous grid independence test (GIT) was carried out comparing coarse (1234 elements), medium (4746 elements) and fine (18400 elements) mesh resolutions. The numerical results were quantitatively accurate in reproducing the expected localised flow acceleration at the contraction and the subsequent boundary layer separation at the expansion. The grid independence study showed stabilisation. The pressure drops were 200.28 Pa, 192.92 Pa and 198.24 Pa for coarse, medium and fine grids respectively. The 198.24 Pa value is a very accurate grid independent solution with less than 3% marginal deviation between the medium and fine meshes. Finally, the finite volume approach is validated in this study as a robust tool for predicting mechanical energy dissipation in variable area piping system.

1. Introduction

In many engineering fields, such as fluid distribution networks, valves, and chemical processing systems [1], internal fluid flows are common that are suddenly changed in cross-sectional area. When a fluid goes through a sudden narrowing and then a sudden widening, it has complicated internal

* *Corresponding author.*
E-mail address: iszat@uthm.edu.my

https://doi.org/10.37934/sjotfe.9.1.112a

dynamics. These include severe flow separation, the formation of recirculation zones, and large losses of mechanical energy [2]. It is very important for engineers to understand and predict these behaviours because the resulting pressure drops directly affect the amount of pumping power needed and the overall energy efficiency of the system [3,4].

A lot of research has been done in the past to quantify the pressure losses due to singular geometric changes. The numerical investigations of Kaushik *et al.,* [5] were carried out to develop basic computational models for water flow through sudden horizontal contraction and expansion using a finite volume discretisation method. Their results showed that special turbulence tracking is needed at the sudden geometric edges for the accurate pressure drop. Recent computational work of Gopal [6] using 2D planar meshes based on this has highlighted the importance of expansion ratios on flow separation and that rigorous grid independence is essential for accurate prediction of pressure drop.

Moreover, Dehkordi *et al.,* [7] measured the high energy dissipation, using the S-A turbulence model. The results showed large areas of low pressure induced by sudden-expansion pipelines for different Reynolds numbers. While the basic physics of isolated expansion and contraction are well understood, the combined aerodynamic effects of successive cross-sectional transitions are mathematically complicated to predict due to the interacting boundary layers [8,9].

2. Methodology

2.1 Pipe Geometry

The geometry adopted in this work is a horizontal pipe with sudden contraction followed by sudden expansion. To shorten the computation times and retain the main flow results, the model was simplified to a 2D planar domain. The total length of the pipe set-up is 190 mm. The geometry consists of three main sections: an upstream large diameter pipe with a length of 45 mm and a height of 40 mm, a narrow contraction throat section with a height of 10 mm and a length of 100 mm, and a downstream expansion pipe that returns to a height of 45 mm with a length of 40 mm. The dimensions were chosen to produce large regions of flow separation and recirculation at the sharp geometric steps. The 2D geometry layout is shown in Figure 1.

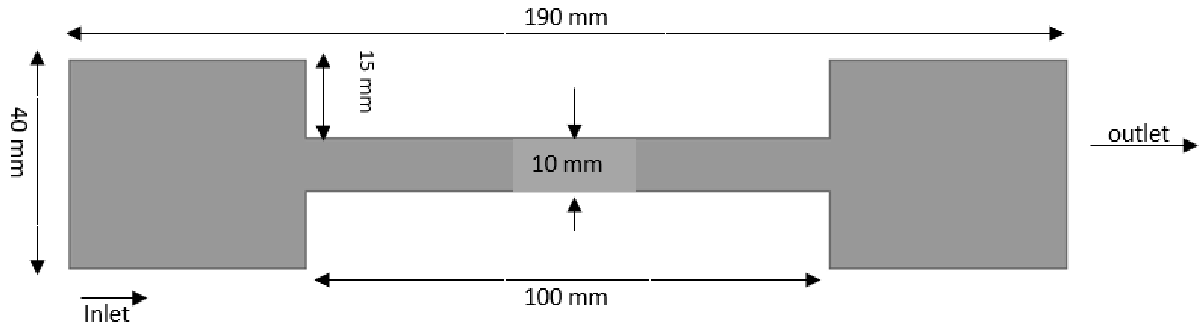

Fig. 1. 2D sudden contraction and expansion pipe geometry

2.2 Meshing Model

The whole 2D fluid domain was discretised using a highly structured grid as seen in Figure 2. The solution settings were selected to have a Quad Dominant sheet body technique in order to make sure the elements are mostly high-quality quadrilateral shapes. This structured layout is favoured to triangular elements because the faces of the cells align nicely with the major direction of the flow, thereby greatly minimising the mistakes of numerical diffusion.

To appropriately address the flow features, precise grid controls were applied in the outline tree using the Face Sizing and local Refinement commands. Therefore, the mesh squares are clearly compressed and are more concentrated in the sharp corners of both the sudden contraction and sudden expansion steps. This local clustering is important since it allows the solver to accurately capture the steep velocity gradients, the boundary layer detachment and the turbulent recirculation eddies that develop immediately downstream of the geometry transitions. If the grid were left coarse in these high velocity regions the software would smooth out the pressure decrease unphysically.

Fig. 2. Computational mesh of pipe in sudden contraction and expansion

2.3 Boundary Conditions

Some boundary conditions were applied on the outside boundaries of the 2D computational domain to properly replicate the fluid flowing into and out of the real pipe network. These settings define the interaction of the fluid with the geometry in a physical sense, and are necessary to solve the governing equations [10]. Figure 3 offers a graphic summary of where these boundaries are employed. Three primary types of boundaries were defined for this steady-state simulation:

i. Inlet: The far-left hand border (shown by the blue arrows) was set as a Velocity-Inlet. The major purpose of the present work is to evaluate the effect of the flow speed, so three different uniform velocities (0.100 m/s, 0.125 m/s and 0.150 m/s) were used here for the parametric analysis.
ii. Outlet: The far-right hand limit (shown by the red arrows) was set as a Pressure-Outlet. The static pressure was set to 0 Pa gauge pressure. This is a common CFD approach which allows the water to depart freely without any artificial back pressure obstructing the flow, similar to a discharge into the open atmosphere [11].
iii. Walls: The Stationary Walls were used to define the top and bottom solid borders of the complete pipe shape (green zones). These edges were mathematically constrained to obey the conventional no-slip criterion. This means that the velocity of the water directly on the wall surface is strictly zero, due to the viscous friction. The software is therefore able to correctly calculate shear stresses and boundary layer development [12].

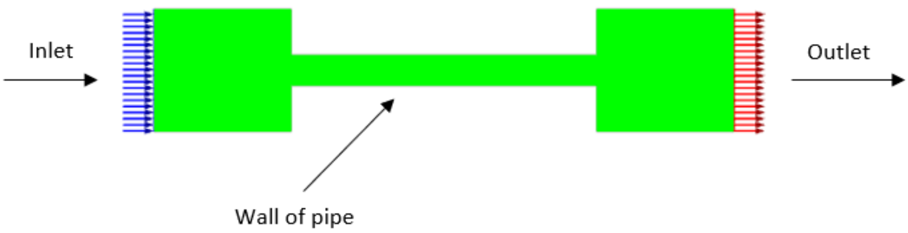

Fig. 3. Boundary condition pipe in sudden contraction and expansion

2.4 Reynolds Number Calculations

At the inlet section, the Reynolds number (Re) was calculated in a dimensionless form to validate the particular flow regime of the fluid in the channel. This number is necessary to calculate the total flow behaviour by mathematically connecting the incoming fluid speed, typical pipe dimension and physical features of the working fluid [13]. In this study, the flow regime is important to understand the strength of pressure decreases and behaviour of flow separation zones at the geometric steps [2,14]. The mathematical expression for the internal flow of pipe is given in Eq. (1):

$$Re = \frac{\rho V D}{\mu} \tag{1}$$

where:
- ρ is the density of water (998.2 kg/m^3)
- V is the fluid speed at the inlet (m/s)
- D is the initial pipe diameter or height (0.04 m)
- μ is the dynamic viscosity of water (0.001003 kg/m.s)

The Reynolds number is calculated using the baseline inlet speed of 0.125 m/s and is determined to be 4,976. This figure is higher than the typical limit of 4,000 for pipe flows, confirming that the flow is totally turbulent. Therefore, a turbulence model must be enabled in the software settings.

2.5 Governing Equations

Numerical calculations in the domain are performed solving the basic transport laws governing conservation of mass, momentum and energy across the grid nodes. The working fluid is incompressible water and the solver solves a particular set of equations from classical computational fluid dynamics literature [10,15] for stable, steady-state conditions. The Conservation of Mass equation (or the Continuity equation) prevents any unphysical mass generation or loss [15] and is written as Eq. (2):

$$\nabla * v = 0 \tag{2}$$

where V is the multi-dimensional velocity vector field. The Conservation of Momentum equation that describes the Navier-Stokes formulation describes the balance between inertial, pressure and viscous forces [16]. This is expressed as Eq. (3):

$$\rho(v.\nabla)V = -\nabla p + \mu \nabla^2 v \tag{3}$$

where p is the static pressure field operating in the pipe. The equation for conservation of energy is solved to account for changes of internal energy due to shear friction and local pressure drops occurring at the steps [10] and is expressed as Eq. (4):

$$\rho C_p (V \cdot \nabla T) = k \nabla^2 T \tag{4}$$

where C_p is the specific heat capacity, T is the local fluid temperature and k is the thermal conductivity of the fluid.

2.6 Convergence and Solution

The steady-state was numerically simulated with the pressure-based finite volume solver embedded in ANSYS Fluent [10]. The standard k-ε closure model [9] was implemented in order to correctly resolve the features of the turbulent core and the recirculation eddies that are formed downstream of the contraction and expansion steps (Figure 4). The pressure-velocity coupling was achieved using the semi-implicit SIMPLE algorithm [13]. Furthermore, the second order upwind spatial discretisation schemes were employed for the momentum and energy equations to acquire the highest calculation accuracy and to decrease the numerical diffusion errors [17]. The calculation domain was initialised with uniform values directly from the inlet boundary parameters. The solver tracking was continuously performed by monitoring the residual history plots until they successfully dropped below the convergence criteria thresholds, which were defined as 10^{-3} for the continuity and velocity components, and 10^{-6} for the energy equation [10]. The solution was in stable convergence in less than 200 iterations for all test cases providing reliable predictions of the localised pressure fields [5,6].

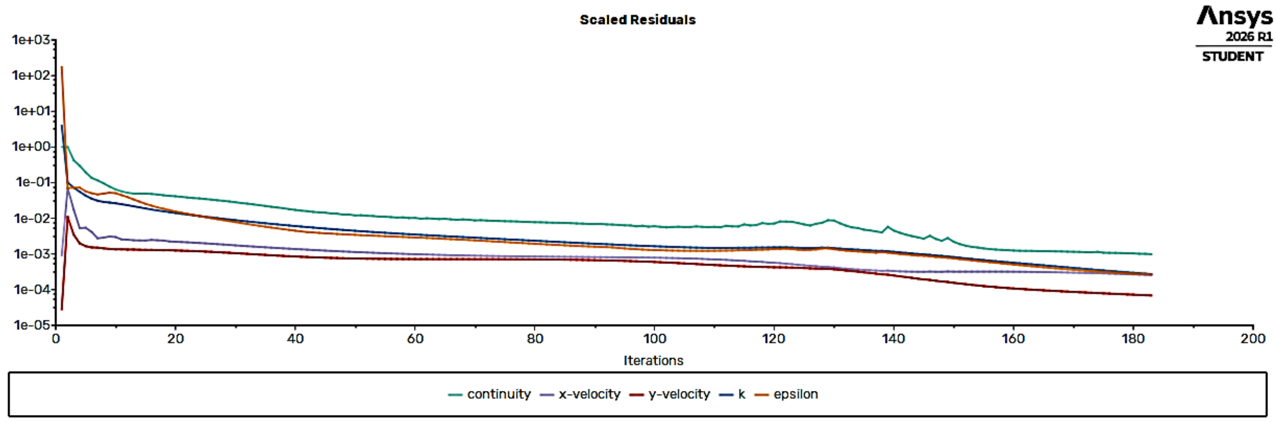

Fig. 4. Convergence monitoring plots (scaled residuals)

3. Results

3.1 Grid Independence Test (GIT)

Before the main simulations, a grid independence study was performed in order to guarantee that the size of the mesh has no effect on the accuracy of the final calculations. We have used the baseline inlet velocity of 0.125 m/s and tested three different meshes namely Coarse, Medium and Fine. The main parameter used for the comparison of the three grids was the total pressure drop over the whole pipe assembly. Table 1 summarises the results of this study. As seen in Table 1, the total calculated pressure drop varies slightly from 200.28 Pa for the Coarse mesh down to 192.92 Pa for the Medium mesh, before finally settling at 198.24 Pa for the Fine mesh. This non-monotonicity can be mostly attributed to the local face scaling and mesh refinement controls imposed at the acute geometric transitions.

When the global cell size is decreased, the re-organization of elements around the sudden contraction and expansion steps modifies the way the solver captures strong localised gradients and sites of downstream flow detachment. An axial data extraction line, named “Line 1”, was fabricated to monitor these localised internal variations along the flow path on a continuous basis. Figure 5 shows Line 1, which is a line straight down the centerline axis of the geometry from inlet (X = 0 m) to outlet (X = 0.15 m).

Table 1
Grid independence study results

Mesh type	Number of elements	Calculated pressure drop (Pa)	Relative error (%)
Coarse	1234	200.28	-
Medium	4746	192.92	3.67
Fine	18400	198.24	2.76

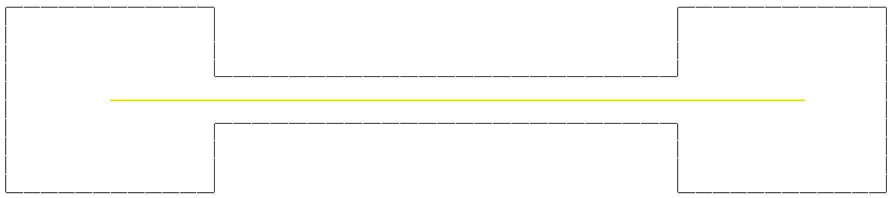

Fig. 5. Location line 1 and plane 1

Figure 6 shows the local static pressure profile obtained along Line 1 for the three mesh configurations. The graph correctly captures the physical features of the fluid flow, showing a constant pressure in the upstream region, a sudden pressure drop exactly at the sudden contraction step (X = 0.025 m), and then a clear pressure recovery and stabilisation region.

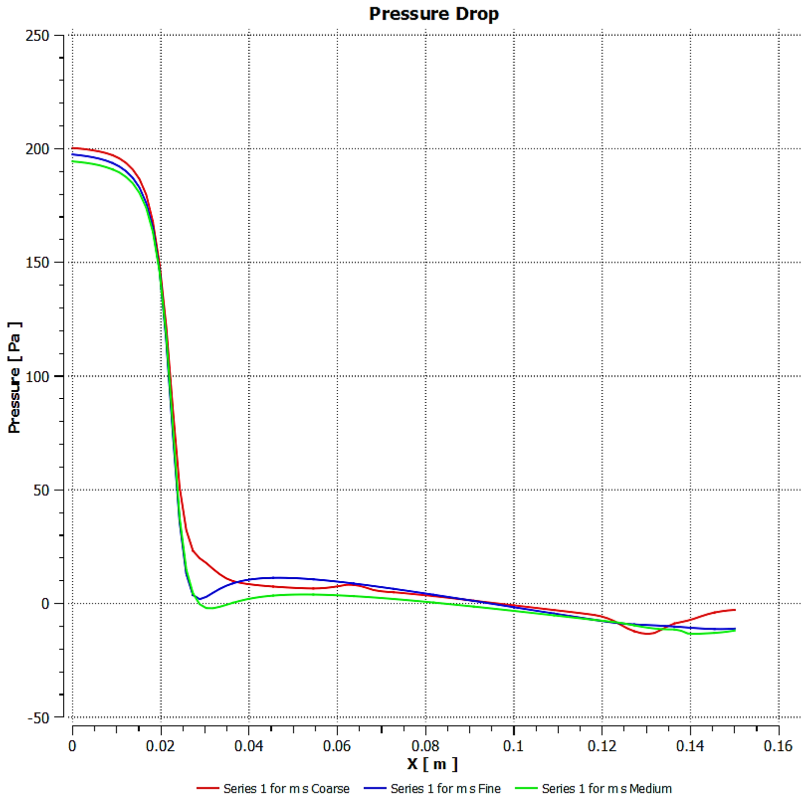

Fig. 6. Pressure drop along the pipe centerline for different mesh densities for GIT

The spatial distribution curves for the Medium and Fine meshes overlap closely for the whole length of the pipe, while the trend for the Coarse mesh shows visible local deviations in the low-pressure zone after the contraction step. The visual convergence shows that the global pressure field is not much affected by further refinement of the grid beyond the medium density.

In quantitative terms the relative error values are low for all transitions. They decrease to 2.76% in transition to the finest grid. Given that the relative variance between the Medium and Fine mesh designs is well within the widely accepted engineering threshold of 5%, the medium mesh with 4,746 elements was selected as the operational grid for all subsequent simulations. This selection allows an optimisation of the trade-off between superfluous computational time and cost and high spatial accuracy.

3.2 Reynolds Number Comparison

A parametric analysis was performed to compare hydrodynamic effects with three input velocities of 0.100 m/s, 0.125 m/s and 0.150 m/s. The associated Reynolds numbers, convergence data and pressure drops across the rapid contraction and expansion pipe assembly are provided in Table 2.

Table 2
Reynolds number and pressure drop comparison results

Inlet velocity (m/s)	Reynolds number	Iterations to converge	Pressure drop
0.1	3992	174	63.62
0.125	4990	165	104.00
0.15	5988	183	144.56

As seen in Table 2, the pressure drop rose considerably from 63.62 Pa to 144.56 Pa with the increase of the Reynolds number from 3,992 to 5,988. This trend is attributed to the fact that the increased inlet velocity immediately increases the flow momentum, turbulence intensity and the frictional resistance along the internal pipe walls [3,4]. Furthermore, all three simulation instances converged successfully within less than 200 iterations, an indication for a highly stable numerical setup.

The relationship between the Reynolds number and the pressure drop indicates that at higher Reynolds numbers, forcing a bigger amount of fluid through the rapid contraction step causes a considerably more severe flow restriction, resulting in higher localised energy losses [20]. Thus, a significantly larger total pressure differential is necessary to force the fluid entirely through the rapid contraction and expansion assembly [2,7]. To further constantly monitor these hydrodynamic differences along the flow route, the local static pressure profiles were obtained along the centerline of the pipe assembly (from inlet X = 0 m to outlet X = 0.15 m) for all three velocities. The obtained space distribution of the pressure is shown in Figure 7.

The hydrodynamic trend, as can be shown in Figure 8, is mathematically comparable for all the three velocity profiles. In the upstream region the static pressure is still rather high and drops sharply and abruptly at the sudden contraction step (X = 0.025 m). The graph is a visual description of the numerical data shown in Table 2. As seen in the graph, the initial pressure required to drive the flow increases sharply with the increase of the inlet velocity. The highest velocity example is represented by the highest curve and shows the most severe pressure gradient at the contraction. This indicates clearly that localised flow resistance and momentum losses at geometric transitions depend strongly on the Reynolds number, scaling aggressively with increasing flow velocity [1,2].

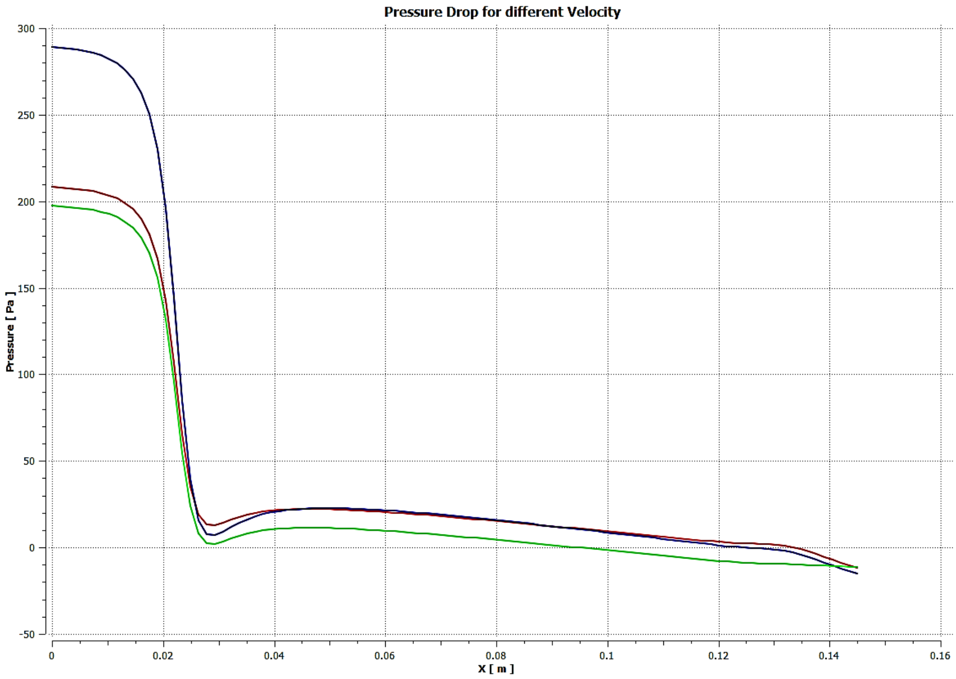

Fig. 7. Pressure distribution along the pipe centerline for different inlet velocities

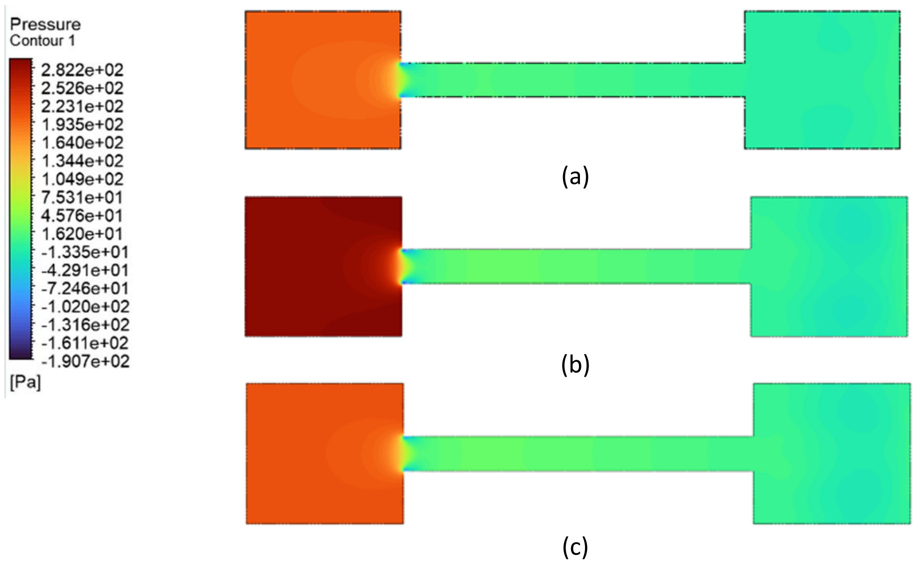

Fig. 8. Static pressure contour comparison across the mid-plane symmetry for (a) 0.100 m/s (b) 0.125 m/s (c) 0.150 m/s operating conditions

3.3 Pressure Distribution

The static pressure contour comparison for the three operating inlet velocities (0.100 m/s, 0.125 m/s, and 0.150 m/s) is illustrated across the mid-plane symmetry cutting section in Figure 8. This comparative visualization is used to analyze the global pressure fields, localized hydraulic resistance, and spatial head loss variations caused by the sudden contraction and expansion steps. As can be seen in Figure 8, the three simulation cases present a very consistent hydrodynamic pressure topology. The maximum static pressure is limited to the inlet area of the upstream wide section of the pipe. This higher-pressure field is the total mechanical energy required to overcome the total downstream fluid skin friction along the pipe walls and the harsh form drag imposed by the geometric restrictions [12,18]. A direct comparison between the three velocity cases shows a clear increase of the pressure field at the upstream inlet with increasing Reynolds number. The 0.100 m/s low-velocity case has the least pressure differential, which requires a visibly lower upstream pressure, shown by the softer orange and yellow contours, to drive the flow. In the opposite cases of baseline and high velocity cases (0.125 m/s and 0.150 m/s) the colour intensity increases at the inlet zone, reaching the deep red contours for the highest velocity. This is a visual confirmation of the numerical trends established in Table 2 and the centerline graph in Figure 7, which shows higher mass flow rates require an aggressively scaled driving pressure force to overcome system resistance [1].

At the sudden contraction plane (X=0.025 m) the flow exhibits a strong crowding of pressure gradients. There is a sharp transition from warm high-pressure contours to a uniform lower-pressure band within the constricted throat. This sudden decrease is a major local head loss because of rapid conversion of static pressure energy into kinetic energy due to strong acceleration of the stream of fluid into the narrow passage [19,20].

In the narrow throat section, a continuous linear pressure drop occurs due to continuous viscous shearing along the internal pipe walls [3,4]. As it exits the throat and enters the sudden enlargement section on the right, the pressure falls to its absolute minimum values. This region (indicated by the lighter blue and green transitions in the vicinity of expansion corners) reflects localised low-pressure zones due to severe flow separation and energy dissipation in the violent recirculation eddies [7,21]. Further downstream a small pressure recovery can be observed as the central fluid jet diffuses and deposits momentum to the surrounding fluid and stabilises to the outlet boundary condition of 0 Pa gauge pressure.

3.4 Velocity Distribution

Figure 9 shows the comparison of the velocity magnitude contours for the three operating inlet velocities (0.100 m/s, 0.125 m/s and 0.150 m/s) over the mid-plane symmetry cutting section. Such a comparative visualisation is essential to evaluate the internal hydrodynamic development, the flow acceleration and the jet diffusion features across the sudden geometric transitions.

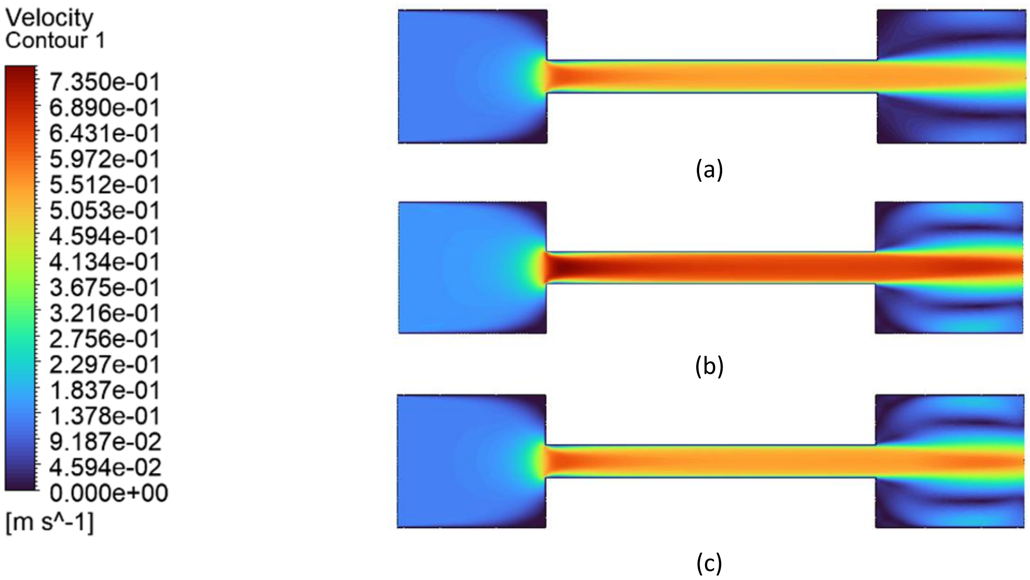

Fig. 9. Velocity magnitude contour comparison across the mid-plane symmetry (a) 0.100 m/s (b) 0.125m/s (c) 0.150m/s operating conditions

As shown in all three simulation cases in Figure 9, the fluid enters the upstream wider pipe section with a low and uniform velocity profile. The available cross-sectional area of flow is severely limited when approaching the sudden contraction step (X = 0.025 m). The fluid is forced to accelerate rapidly when it reaches the narrow throat section [1] in strict observance of the basic principle of mass conservation. The violent acceleration generates a high-speed central core, visualised by the prominent red and orange contour zones, where the fluid reaches its absolute maximum velocity. A direct comparison among the three velocity conditions shows a linear proportional relationship, meaning that as the inlet velocity increases, the maximum core velocity within the throat increases proportionally, keeping the continuity equation mathematically intact [1].

When the high momentum fluid jet enters the sudden expansion, it cannot expand instantaneously to fill the larger diameter of the downstream pipe [6]. Consequently, the flow separates abruptly at the expansion corners and forms a concentrated central jet, which slowly diffuses along the pipeline [21]. The dark blue regions correspond to near zero or very low velocity flow, and clearly delineate the stagnation and recirculation zones around the central high velocity jet. The comparative contours show that at higher inlet velocities, this central jet has much higher kinetic energy, and therefore needs a longer axial distance in order to be completely dissipated in momentum and to reattach to the downstream pipe walls.

Numerical results in general show that increase of the input velocity and therefore the Reynolds number causes a large increase of the overall pressure drop across the abrupt contraction and expansion pipe assembly. The example with the maximum flow velocity (0.150 m/s) yields the maximal mass transport rate through the system, but causes severe flow separation, large turbulent recirculation zones during the abrupt expansion and the largest hydraulic resistance penalty of 144.56 Pa. The lowest velocity scenario (0.100 m/s) had a total pressure drop of 63.62 Pa, lowest of the cases considered, but limited the overall fluid flow, which may not be suitable for practical industrial pipeline applications. Therefore, the most balanced and optimised baseline operating state for the geometry is 0.125 m/s. It can provide a moderate and stable fluid transport rate with a highly acceptable pressure drop of 104.00 Pa, which can balance the system hydrodynamic performance and pumping power efficiency well.

4. Conclusions

In this study, Computational Fluid Dynamics (CFD) analysis was successfully conducted to explore the internal hydrodynamic behaviour of water moving inside a two-dimensional rapid contraction and expansion pipe assembly. A parametric study was carried out at three different inlet velocities (0.100 m/s, 0.125 m/s, and 0.150 m/s) to study the impacts of rising Reynolds numbers on the internal flow development, the pressure distribution in space, and the localised energy losses. The numerical model was quite stable. All the runs of the simulation converged in less than 200 iterations, which confirmed the trustworthiness of the computational framework.

The simulation findings indicated a direct and significant relationship between the operating velocity and the hydraulic resistance produced. The total pressure drop across the system increased aggressively from 63.62Pa to 144.56Pa as the Reynolds number moved from 3992 into the turbulent regime at 5988. The pressure and velocity contour analyses verified that these large head losses were primarily caused by two distinct geometric effects, namely the sudden contraction step where the flow accelerates rapidly and the static pressure is converted into kinetic energy and the sudden expansion step where the flow separates severely. The abrupt expansion led to the formation of concentrated central jets of fluid with prominent low pressure recirculation eddies in the downstream corners which served as substantial sources of mechanical energy dissipation.

Finally, our work finds that while greater inlet velocities maximise the mass transfer rate, they impose severe hydrodynamic penalties and require much higher pumping power to overcome the turbulent form drag. Based on the comparison study, it was shown that the intermediate velocity of 0.125 m/s at the intake was the best working condition for this particular pipe geometry. This arrangement offers a very effective balance, providing a consistent fluid throughput while maintaining a moderate and efficient total pressure drop of 104.00 Pa.

References

[1] Frank M. White. *Fluid Mechanics*. McGraw Series in Mechanical Engineering.

[2] Benedict, Robert P., N. A. Carlucci, and S. D. Swetz. "Flow losses in abrupt enlargements and contractions." *Journal of Engineering for Gas Turbines and Power* 88, no. 1 (1966): 73-81. https://doi.org/10.1115/1.3678482.

[3] Moody, L. F. (1944). Friction factors for pipe flow. *Transactions of the American Society of mechanical engineers*, *66*(8), 671-678. https://doi.org/10.1115/1.4018140

[4] Colebrook, Cyril Frank, T. Blench, H. Chatley, E. H. Essex, J. R. Finniecome, G. Lacey, J. Williamson, and G. G. Macdonald. "Correspondence. turbulent flow in pipes, with particular reference to the transition region between the smooth and rough pipe laws (includes plates)." *Journal of the Institution of Civil engineers* 12, no. 8 (1939): 393-422. https://doi.org/10.1680/ijoti.1939.13150

[5] Kaushik, V. V. R., Sumana Ghosh, Gargi Das, and Prasanta Kumar Das. "CFD simulation of core annular flow through sudden contraction and expansion." *Journal of Petroleum Science and Engineering* 86 (2012): 153-164. https://doi.org/10.1016/j.petrol.2012.03.003

[6] Gopal, Arul Nalmanan Raja. "Comparative study of internal flow dynamics using CFD for of sudden expansion pipe." *Journal of Advances in Fluid, Heat, and Materials Engineering* 5, no. 1 (2025): 37-44. https://doi.org/10.37934/afhme.5.1.3744a

[7] Dehkordi, P. Babakhani, A. Azdarpour, and E. Mohammadian. "The hydrodynamic behavior of high viscous oil-water flow through horizontal pipe undergoing sudden expansion—CFD study and experimental validation." *Chemical Engineering Research and Design* 139 (2018): 144-161. https://doi.org/10.1016/j.cherd.2018.09.026

[8] Wilcox, David C. *Turbulence modeling for CFD*. Vol. 2. La Canada, CA: DCW industries, 1998.

[9] Launder, Brian Edward, and Dudley Brian Spalding. "The numerical computation of turbulent flows." In *Numerical Prediction Of Flow, Heat Transfer, Turbulence And Combustion*, pp. 96-116. Pergamon, 1983.

[10] Dick, Erik. "Introduction to finite volume methods in computational fluid dynamics." In *Computational Fluid Dynamics*, pp. 275-301. Berlin, Heidelberg: Springer Berlin Heidelberg, 2009. https://doi.org/10.1007/978-3-540-85056-4_11

[11] Dehkordi, P. Babakhani, A. Azdarpour, and E. Mohammadian. "The hydrodynamic behavior of high viscous oil-water flow through horizontal pipe undergoing sudden expansion—CFD study and experimental validation." *Chemical Engineering Research and Design* 139 (2018): 144-161. https://doi.org/10.1016/j.cherd.2018.09.026

[12] Wu, Kunyi, Bo Lei, Yanhua Qiu, Hui Li, Shize Wei, Feng Wang, Yu Wu, and Liming Zhang. "Analysis of In-Station Pressure Drops in Shale Gas Gathering Systems Using CFD and Network Modeling." *Fluid Dynamics & Materials Processing* 22, no. 2 (2026). https://doi.org/10.32604/fdmp.2026.076662

[13] Patankar, Suhas. *Numerical Heat Transfer and Fluid Flow*. CRC press, 2018. https://doi.org/10.1201/9781482234213

[14] Patankar, Suhas V., and D. Brian Spalding. "A calculation procedure for heat, mass and momentum transfer in three-dimensional parabolic flows." In *Numerical Prediction of Flow, Heat Transfer, Turbulence and Combustion*, pp. 54-73. Pergamon, 1983. https://doi.org/10.1016/0017-9310(72)90054-3

[15] Blazek, Jiri. *Computational fluid dynamics: principles and applications*. Butterworth-Heinemann, 2015. https://doi.org/10.1016/B978-0-08-099995-1.00012-9

[16] Durst, F., and T. Loy. "Investigations of laminar flow in a pipe with sudden contraction of cross sectional area." *Computers & fluids* 13, no. 1 (1985): 15-36. https://doi.org/10.1016/0045-7930(85)90030-1

[17] Shih, Tsan-Hsing, William W. Liou, Aamir Shabbir, Zhigang Yang, and Jiang Zhu. "A new k-ϵ eddy viscosity model for high reynolds number turbulent flows." *Computers & Fluids* 24, no. 3 (1995): 227-238. https://doi.org/10.1016/0045-7930(94)00032-t

[18] Bandarra Filho, Enio Pedone, Erick Oliveira do Nascimento, Muhammad Farooq, and Luben Cabezas-Gómez. "Numerical investigation on heat transfer and pressure drop in silver/water nanofluids flowing through tubes with variable expansion–contraction ratios." *Energies* 18, no. 1 (2025): 161. https://doi.org/10.3390/en18010161

[19] Choi, Sung-Woong, Hyoung-Seock Seo, and Han-Sang Kim. "Analysis of flow characteristics and effects of turbulence models for the butterfly valve." *Applied Sciences* 11, no. 14 (2021): 6319. https://doi.org/10.3390/app11146319

[20] Fester, Veruscha, Baudouin Mbiya, and Paul Slatter. "Energy losses of non-Newtonian fluids in sudden pipe contractions." *Chemical Engineering Journal* 145, no. 1 (2008): 57-63. https://doi.org/10.1016/j.cej.2008.03.003

[21] Durst, F., J. C. F. Pereira, and C. Tropea. "The plane symmetric sudden-expansion flow at low Reynolds numbers." *Journal of Fluid Mechanics* 248 (1993): 567-581. https://doi.org/10.1017/S0022112093000916